

AN X-RAY AND OPTICAL LIGHT CURVE MODEL OF THE ECLIPSING SYMBIOTIC BINARY SMC3

MARIKO KATO

Department of Astronomy, Keio University, Hiyoshi, Yokohama 223-8521, Japan;

IZUMI HACHISU

Department of Earth Science and Astronomy, College of Arts and Sciences, University of Tokyo, Komaba, Meguro-ku, Tokyo 153-8902, Japan

AND

JOANNA MIKOŁAJEWSKA

N. Copernicus Astronomical Center, Bartycka 18, 00-716 Warszawa, Poland

to appear in the Astrophysical Journal

ABSTRACT

Some binary evolution scenarios to Type Ia supernovae include long-period binaries that evolve to symbiotic supersoft X-ray sources in their late stage of evolution. However, symbiotic stars with steady hydrogen burning on the white dwarf's (WD) surface are very rare, and the X-ray characteristics are not well known. SMC3 is one such rare example and a key object for understanding the evolution of symbiotic stars to Type Ia supernovae. SMC3 is an eclipsing symbiotic binary, consisting of a massive WD and red giant (RG), with an orbital period of 4.5 years in the Small Magellanic Cloud. The long-term V light curve variations are reproduced as orbital variations in the irradiated RG, whose atmosphere fills its Roche lobe, thus supporting the idea that the RG supplies matter to the WD at rates high enough to maintain steady hydrogen burning on the WD. We also present an eclipse model in which an X-ray emitting region around the WD is almost totally occulted by the RG swelling over the Roche lobe on the trailing side, although it is always partly obscured by a long spiral tail of neutral hydrogen surrounding the binary in the orbital plane.

Subject headings: binaries: eclipsing – binaries: symbiotic – circumstellar matter – stars: individual (SMC3) – stars: winds, outflows – white dwarfs

1. INTRODUCTION

SMC 3 is a symbiotic star consisting of a massive white dwarf (WD) and an M giant. Its orbital period is about 4.5 years. It is a supersoft X-ray source (SSS) (RX J0048.4–7332) that has been under observation for 20 years (Jordan et al. 1996; Mürset et al. 1997; Kahabka 2004; Kahabka & Haberl 2006; Orio et al. 2007; Sturm et al. 2011, and references therein). The WD appears to be very massive because SMC3 is the strongest X-ray source among symbiotic binaries (Mürset et al. 1997). In addition, a massive WD ($M_{\text{WD}} > 1.18M_{\odot}$) is suggested from the results of X-ray spectrum fittings with model atmospheres (Orio et al. 2007). The 20 years observation period is quite long compared with the durations of the supersoft X-ray phases of classical novae harboring massive WDs, 0.7 years for $1.0 M_{\odot}$, 2.7 years for $0.8 M_{\odot}$, and 8.9 years for $0.6 M_{\odot}$ (see Table 2 in Kato & Hachisu 1994). Therefore, it is very unlikely that SMC3 is a nova remnant. Orio et al. (2007) concluded that SMC3 is a symbiotic binary with a steady hydrogen-shell-burning WD because no nova outbursts have been recorded in the last 50 years despite continuous optical monitoring of the SMC.

Steady hydrogen-shell-burning WDs have attracted attention in relation to Type Ia supernova (SN Ia) progenitors because these WDs accumulate accreted matter, causing their masses to increase. In the single degenerate (SD) scenario to SNe Ia in which an accret-

ing WD grows in mass to reach the Chandrasekhar mass and explodes as an SN Ia, there are two well-known paths of binary evolution (Li & van den Heuvel 1997; Hachisu et al. 1999a,b): one is the main-sequence (MS) channel, for those with an MS companion, and the other is the symbiotic channel, for those with an red giant (RG) companion. In these evolutionary channels, a typical binary evolves in its final stage from the wind phase (steady hydrogen-shell-burning with optically thick winds) through the supersoft X-ray phase (steady hydrogen-shell-burning with no optically thick winds) to the recurrent nova phase (intermittent hydrogen shell burning, e.g., Hachisu et al. 2010). In the symbiotic channel, progenitor binaries are expected to evolve into symbiotic stars with a massive WD with steady hydrogen-shell-burning (Hachisu et al. 2012). They are potentially strong SSSs. If they are detected, we use them as testbeds for the SN Ia progenitor scenarios. Unfortunately, symbiotic X-ray binaries with a massive WD are very rare. SMC3 is one such rare example.

It has been suggested that the supersoft X-ray fluxes of galaxies are much weaker than expected for the SD scenario (Orio et al. 2010; Di Stefano 2010a). Di Stefano (2010b) emphasized that the double degenerate (DD) scenario for SNe Ia, in which two WDs merge and then explode as an SN Ia, predicts a large number of symbiotic stars before the second common envelope evolution that produces a DD system. Therefore, the lack of supersoft X-ray flux is a problem common to both SD and DD scenarios. Gilfanov & Bogdán (2010) claimed that

weak supersoft X-ray emission in early-type galaxies is negative evidence against the SD scenario. Orio et al. (2010) pointed out that most SSSs in M31 are transient, and steady-burning sources are rare, possibly because of low duty cycles of the SSS phases in these sources. The work by Gilfanov & Bogdán (2010) was also criticized by Hachisu et al. (2010), Kato (2012), and Wang & Han (2012), because Gilfanov & Bogdán adopted not only overestimated numbers of expected SSSs but also unrealistically large X-ray fluxes for symbiotic SSSs. If we use a reliable number of symbiotic SSSs based on the SD scenario (Hachisu et al. 1999a) and realistic X-ray fluxes, we can statistically explain the weak supersoft X-ray emission in early-type galaxies, consequently, this strongly supports the SD model as a promising scenario for SNe Ia (Hachisu et al. 2010). Dilday et al. (2012) reported a detailed spectral analysis of the SN Ia PTF 11kx and concluded that it had a symbiotic nova progenitor, mainly because of a complex circumstellar environment. Chiotellis et al. (2012) also suggested that Kepler’s SN (SN 1604) is Type Ia, and its progenitor was a symbiotic star consisting of a WD and an asymptotic giant branch (AGB) star because of strong interaction with circumstellar matter.

However, the nature of symbiotic steady-burning X-ray sources are yet to be fully understood; for example, their WD masses, RG companion masses, spectral types, orbital periods, wind mass-loss rates from both stars, and nebular emissions, as well as their origins and evolutionary paths to the present binary state. In symbiotic stars, a hot WD may be embedded in a RG’s cool wind that obscures supersoft X-rays (Hachisu et al. 2010; Kato 2012; Nielsen et al. 2012). For example, V407 Cyg, a symbiotic classical nova, showed a very weak supersoft X-ray flux in the later phase of its 2010 outburst because the WD is deeply embedded in a thick envelope originating from the cool giant wind (Schwarz et al. 2011; Nelson et al. 2012; Hachisu & Kato 2012). Interestingly, strong symbiotic SSSs have been discovered so far only in the galactic halo (AG Dra) or in the Small Magellanic Cloud (SMC3 and Lin358; Orio et al. 2007). This suggests that a low-metallicity environment is an important clue to the detection of supersoft X-rays from symbiotic systems. To examine such a possibility, we need to study individual symbiotic SSSs in detail.

In symbiotic binaries, a cool wind blows from the RG, and a hot wind blows from the WD. Radiation at various wavelengths may originate from different areas of the binary. Researchers have become interested mainly in SMC3’s X-ray nature, but its binary nature has not yet been fully understood. In relation to binary evolution scenarios to SNe Ia, it is very important to know why the supersoft X-ray fluxes are so weak, although their WDs are believed to be very massive. In this work, we propose a binary model that explains both the long-term V magnitude variations and observed X-ray eclipses. In Section 2, we summarize the observational properties of SMC3 and propose our basic model of it. In Section 3, we present our model light curves for long-term variations in the V magnitude. Section 4 presents our X-ray eclipse light curve model. Discussion and conclusions follow in Sections 5 and 6, respectively.

2. THE MODEL OF SMC3 – A SYMBIOTIC X-RAY SOURCE

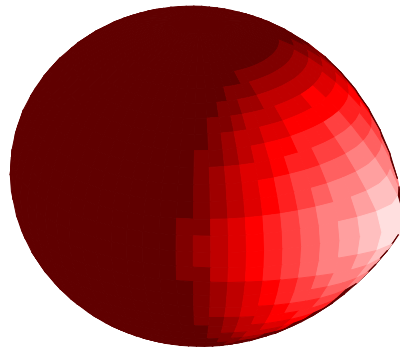


FIG. 1.— Schematic view of the binary in the V band. The RG fills its Roche lobe, and its hemisphere is irradiated by the hot WD (right: black dot). Distribution of the RG’s surface temperature is indicated by red color gradient on a linear scale (white-red side is the highest temperature: 5400 – 5500 K). The temperature of the RG on the non-irradiated side (dark red) is the parameter T_{RG} (3100 – 3500 K). We assume a steady hydrogen-shell-burning WD. The WD and its surrounding hot gas are invisible in the V band because of their high temperature. The RG tail of neutral hydrogen is unseen because it is transparent in the V band.

Morgan (1992) reported low-resolution optical spectra of SMC3. The RG is classified as spectral type M0. The spectrum is typical for a high-excitation s-type symbiotic star and exhibits Balmer, He I, and He II emission lines as well as Raman-scattered O VI 6825 and 7082 features. The spectra also show an [Fe X] emission line, an unusually high ionization line for a symbiotic star. Optical spectra were also published by Mürset et al. (1996) for 1994 Dec 20 – 23 [orbital phase of $\phi = 0.26$, see Equation (2) in Section 3 below for the ephemeris], and by Orio et al. (2007) for 1994 Oct 17 ($\phi = 0.22$). Orio et al. (2007) remarked that coronal lines [Fe IX] and [Fe X] in the optical spectra indicate a photoionizing source at a very high temperature of $T \sim 5 \times 10^5$ K. One *IUE* UV spectrum (SWP 47572L) was taken on 1993 April 30 (JD 2449107.5) (Vogel & Morgan 1994) ($\phi = 0.89$, i.e., X-ray ingress). This spectrum appears typical for a symbiotic star of moderate excitation (Jordan et al. 1996).

Near-infrared (IR) I magnitude light curves (shown later in Figure 3) taken by the OGLE II and III projects show an irregular variation with a period about 110 days (Kahabka 2004; Sturm et al. 2011), which is attributed to pulsation of the RG by Kahabka (2004). A blue filter light curve was secured by the MACHO project for as long as 6 years (also shown later in Figure 3); it shows a long-term variation with a period of ~ 1600 days similar to the X-ray variation (Kahabka 2004; Sturm et al. 2011), superposed by a short-term variation similar to that of the I magnitude light curve.

Therefore, as a basic model of SMC3, we assume a binary consisting of a massive WD and an irradiated RG as plotted in Figure 1 (which is explained in detail in Section 2.1). Table 1 gives the assumed masses of the WD and RG, the separation a , and the effective radii of the Roche lobes for the RG and WD. Here the binary separation a is calculated from Kepler’s third law, $a^3 = G(P_{\text{orb}}/2\pi)^2(M_{\text{WD}} + M_{\text{RG}})$, assuming a circular orbit and $P_{\text{orb}} = 1634$ days (as determined in Section 3).

2.1. The RG Component

Near-IR photometry of SMC3 is reported as $\langle J \rangle = 11.935$, $\langle H \rangle = 11.035$, and $\langle K_s \rangle = 10.8$ at JD 2451034.7

TABLE 1
 BINARY PARAMETERS^a

WD mass (M_{\odot})	RG mass (M_{\odot})		a (R_{\odot})	$R_{\text{RL}}(\text{RG})^{\text{b}}$ (R_{\odot})	$R_{\text{RL}}(\text{WD})^{\text{c}}$ (R_{\odot})
1.35	3.0	...	953	428	298
1.35	2.0	...	873	361	302
1.35	1.5	...	828	321	306
1.35	1.0	...	776	274	314
1.35	0.8	...	753	252	320
1.35	0.6	...	729	227	329
1.35	0.4	...	703	197	342
1.20	0.8	...	735	253	305
1.10	0.8	...	723	254	294
1.00	0.8	...	710	255	283

^a We assume $P_{\text{orb}} = 1634$ days and a circular orbit.

^b Effective Roche lobe radius of the RG (Eggleton 1983)

^c Effective Roche lobe radius of the WD (Eggleton 1983)

(Phillips 2007) (hereafter $K_s = K$). This date is close to mid-eclipse, $\phi = 0.07$. These JHK magnitudes represent the RG magnitudes well. Then, we obtain reddening-corrected magnitudes of $J_0 = 11.848$, $H_0 = 10.977$, and $K_0 = 10.765$ with $A_J = 0.874 \times E(B - V) = 0.087$, $A_H = 0.589 \times E(B - V) = 0.058$, and $A_K = 0.353 \times E(B - V) = 0.353 \times 0.099 = 0.035$. Here we use the extinction coefficients given by Cardelli et al. (1989) and the extinction $E(B - V) = 0.099$ given by Hilditch et al. (2005). In our light curve fittings, on the other hand, the RG magnitudes are obtained from the light curve minimum; i.e., when the RG is in front of the WD, we see the non-irradiated side of the RG. From Figure 3 we get $I \sim 13.34$ and $V \sim 15.35$. Thus, the reddening-corrected magnitude becomes $I_0 = 13.193$ and $V_0 = 15.043$, with $A_I = 1.48 \times 0.099 = 0.147$ and $A_V = 3.1 \times 0.099 = 0.307$ (Cardelli et al. 1989).

The RG luminosity is estimated using the relationship between $BC(K)$ and $(J - K)_0$ obtained for SMC variables (Bessel & Wood 1984),

$$BC(K) = 0.60 + 2.65(J - K)_0 - 0.67(J - K)_0^2, \quad (1)$$

for $0.6 < (J - K)_0 < 1.5$.

We obtain $BC(K) = 2.68$ for $(J - K)_0 = 1.083$. The bolometric magnitude becomes $M_{\text{bol}} = 10.765 + 2.68 - 18.91 = -5.46$, i.e., $L_{\text{bol}} = 12000 L_{\odot}$. Here we use $M_{\text{bol}}(\text{Sun}) = 4.75$ for the absolute bolometric luminosity of the Sun. Bessel & Wood (1984) also presented another relationship, $BC(K)$ vs. $(V - K)_0$, from which we get $BC(K) \sim 2.7$; this is quite consistent with the estimate obtained from Equation (1).

The effective temperature of the RG is estimated using the color-temperature relation of a model atmosphere for low-metallicity RGs given by Kućinskas et al. (2006) together with a metal abundance of $[M/H] = -1$. We get $T_{\text{eff}} \sim 3800$ K for $(J - K)_0 = 1.083$, $T_{\text{eff}} \sim 3600$ K for $(V - K)_0 = 4.278$, and $T_{\text{eff}} \sim 3700$ K for $(V - I)_0 = 1.85$. These color temperatures are consistent with each other within the accuracy of the model temperature (± 100 K). They are also consistent with the spectral type M0 estimated by Morgan (1992) because for Galactic bright giants, the spectral type M0 corresponds to 3700 - 3800 K (Straižys & Kuriliene 1981). The radius of the RG becomes $250 R_{\odot}$ for $T_{\text{eff}} = 3800$ K, $270 R_{\odot}$ for 3700 K, and $280 R_{\odot}$ for 3600 K, with Stefan-Boltzmann's law $L = 4\pi R_{\text{RG}}^2 \sigma T_{\text{eff}}^4$. Comparing these values with the

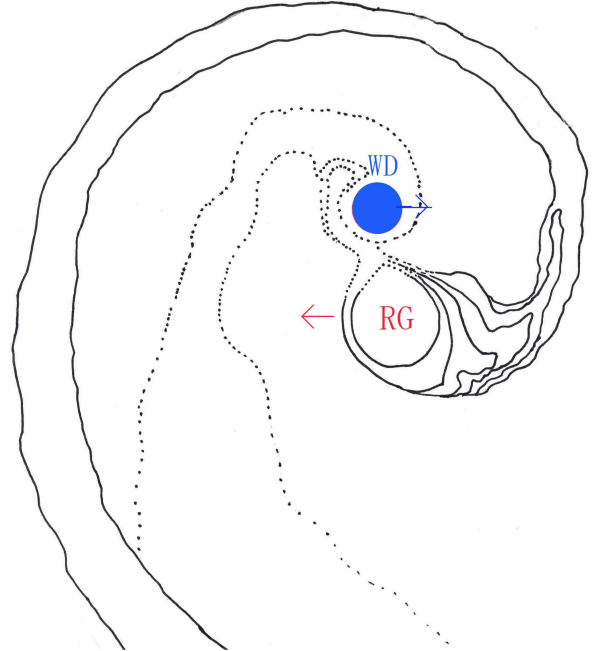


FIG. 2.— Schematic polar view of SMC3. Blue circular region represents a hot ionized plasma centered on the WD that scatters supersoft X-ray photons from the WD. The RG almost fills its Roche lobe and has a large trailing tail of neutral hydrogen that absorbs supersoft X-rays. Arrows denote the orbital motion of each component. Ionized and neutral regions are plotted by dotted and solid lines, respectively. This schematic figure was made using information from numerical calculations (Sawada et al. 1986; Mohamed & Podsiadlowski 2012). Contours denote the density taken from Sawada et al. (1986). Size and shape of each part are not important in our X-ray light curve model except for the height (thickness) from the orbital plane.

 TABLE 2
 LIGHT CURVE MODEL OF X-RAY ECLIPSE

Subject	Model 1	Model 2
Duration of total X-ray eclipse $\Delta\phi$... 0.22	0.19
Duration of total X-ray eclipse (day)	... 363 day	304 day
Delay of X-ray mid-eclipse $\Delta\phi$... 0.075	0.075
Delay of X-ray mid-eclipse (day)	... 123 day	123 day
RG radius	... $245 R_{\odot}$	$199 R_{\odot}$
Minimum height of the tail	... $48 R_{\odot}$	$31 R_{\odot}$
Radius of the hot nebula R_{NE}	... $100 R_{\odot}$	$100 R_{\odot}$

Roche lobe radii in Table 1 (i.e., $252 R_{\odot}$ for a $0.8 M_{\odot}$ RG and $274 R_{\odot}$ for a $1.0 M_{\odot}$ RG), we see that the estimated RG radii are quite consistent with the effective Roche lobe radii of the RG. Thus, we may safely assume a Roche-lobe-filling RG (Figure 1).

The RG is a semiregular variable with a pulsation period of 110 days. SMC3 is located in the upper part of the period - K magnitude diagram for SMC OGLE variables (Ita et al. 2004). In this diagram, SMC3 is located at the border between sequences A^+ and B^+ , both of which are classified as “less regular pulsation AGB variables.” The pulsation mode is probably not fundamental, but is likely the first/second or third overtone. This is consistent with the irregular I band variation with a small amplitude of $\Delta I \sim 0.05$ mag.

2.2. The Hot Component: Supersoft X-ray Source

As briefly introduced in Section 1, SMC3 (=RX J0048.4–7332) is an exceptionally bright SSS among symbiotic stars (see Table 1 in Mürset et al. 1997), and has been observed with *ROSAT*, *Chandra*, and *XMM-Newton* (Jordan et al. 1996; Kahabka 2004; Orio et al. 2007; Sturm et al. 2011, and references therein). Jordan et al. (1996) analyzed *ROSAT* spectra combined with a UV spectrum from *IUE*. They found that a very hot Wolf-Rayet-type model atmosphere fit the spectra reasonably well, but blackbody and hydrostatic plane-parallel models did not. In their analysis, the wind mass-loss rate is several times $10^{-6} M_{\odot} \text{ yr}^{-1}$ and the central stellar surface is hidden by stellar winds. However, they combined the *ROSAT* ($\phi = 0.65$: out of eclipse) and the *IUE* spectrum ($\phi = 0.89$: ingress), which are not simultaneous, so they may have overestimated the wind mass-loss rate in order to reproduce the smaller UV flux (due to the half-eclipsed state) with only the wind absorption.

The supersoft X-ray count rates for SMC3 decreased by a factor of 50 over more than 300 days starting in May 1993 (Kahabka 2004). Kahabka presented a model of this X-ray decrease in which the WD orbits within a massive wind from the RG. The wind is highly ionized but still contains neutral hydrogen. The column density of neutral hydrogen (N_{H}) in the line of sight changes periodically with the orbital motion of the WD. As a result, the X-ray count rate decreases when the WD is on far side as seen from the Earth. Orio et al. (2007) criticized this scenario because this model predicts nebular emission lines at the high mass-loss rate of the RG wind they assumed, but no such lines were observed in the optical spectra. Orio et al. argued that the values of N_{H} appeared to be unchanged or only slightly higher in the 2003 eclipse, which seemed to be consistent with a real eclipse caused by the RG itself, rather than with a significant contribution by additional obscuration caused by an RG wind.

Recently, Sturm et al. (2011) analyze spectra newly obtained with *XMM-Newton* EPIC-pn, using a blackbody model, in both high and low X-ray flux stages. Their spectral fits do not yield good results for a model of changing neutral-hydrogen column density because the spectra in low X-ray flux stages cannot be reproduced. Therefore, Kahabka’s model was not supported. Instead, they suggested Compton scattering by fully ionized matter that is distributed azimuthally unevenly in the orbital plane. This requires the RG cool wind to completely ionize up to the RG surface because the neutral-hydrogen column-density does not increase. However, such a situation is very unlikely because Raman-scattered light was observed (Morgan 1992). Sturm et al. (2011) also suggested a temperature variation model for the eclipse, but this seems to be inconsistent with the light curves. If the temperature varies while the total luminosity remains constant, the V magnitude light curve should be anti-correlated with the X-ray variation, but there is no indication of such behavior. Although these authors misunderstood and rejected, the rest of their models, i.e., the varying emitting area model with constant temperature and column density, corresponds to the “real eclipse,” as Orio et al. (2007) already suggested, and reproduces very well the spectra at both high and low X-ray fluxes.

On the bases of these analyses, we assume that the

WD is embedded in very hot, highly ionized gas that scatters supersoft X-ray photons emitted from the WD. In other words, the X-ray emitting region is not a point source but is substantially extended around the WD, as illustrated by the blue circular region in Figure 2. We also add circumbinary matter distributed as in Figure 2, in which the RG swelling over its Roche lobe has a long spiral tail of neutral hydrogen (see Section 4 for details).

3. LIGHT CURVES OF V AND I VARIATIONS

We assume a binary configuration as in Figure 1 to calculate the V and I light curves. As we already discussed in Section 2.1, it is very likely that the RG almost fills its Roche lobe. We assume a circular orbit with an inclination angle of $i = 90^{\circ}$ and WD and RG masses of $M_{\text{WD}} = 1.0\text{--}1.35 M_{\odot}$ and $M_{\text{RG}} = 0.8\text{--}2.0 M_{\odot}$, respectively. We further assume the RG radius to be constant, although the RG is pulsating as a semiregular variable. This approximation is good if the amplitude of the radius pulsation is small. In the symbiotic nova PU Vul, the companion RG is also a semiregular variable, and the amplitude of its radius pulsation is estimated to be 3–7% by eclipse analysis (Kato et al. 2012). Because the amplitude of V variation in SMC3 (~ 0.15 mag) is much smaller than that in PU Vul (~ 1 mag), a constant RG radius is a good approximation.

The WD has hydrogen shell burning so its surface is hot enough to emit supersoft X-rays. The hemisphere of the RG toward the WD absorbs high-energy photons emitted from the WD, and this side is heated (see Figure 1). The heated surface emits blackbody radiation at a local temperature calculated from the energy balance. In contrast, in the opposite hemisphere, the temperature remains low at the original surface temperature, T_{RG} , which we take as a parameter. We neglected the temperature change due to RG pulsation. The RG surface is divided into small patches ($N = N_r \times N_{\theta} = 64 \times 32$) and the energy balance is calculated at each patch to obtain its local temperature. Then, we sum them up to obtain the total V and I magnitudes of the RG at a specified orbital phase. A detailed description of our calculation method is given in Hachisu & Kato (2001).

The WD and its hot thin nebula (blue region in Figure 2) are extremely hot ($T \sim 5 \times 10^5$ K; Orio et al. 2007), so their emission contributes little to the V and I bands. We considered the hot nebula surrounding the WD to be optically thin (see the discussion in Section 5), so it is transparent in the I and V bands. We also assumed that the spiral tail is neutral and transparent in these I and V bands, as described in Section 4.2.

However, the cool tail may contribute to the I magnitude. As the standard model in this work, we determined the original RG temperature (i.e., that of the non-irradiated surface) by fitting our V model light curves with the observed V magnitude. The resulting I light curve is darker than the observed one and does not fit well, as seen below. Therefore, we added a nebular contribution in the I band in order to fit our model light curve with the observed I band light curve. We suppose that this nebular contribution is due mainly to the cool RG tail.

We assumed a steady hydrogen-shell-burning WD of bolometric luminosity $L_{\text{WD}} = 3.77 \times 10^4 L_{\odot}$ for $M_{\text{WD}} = 1.35 M_{\odot}$, $L_{\text{WD}} = 3.59 \times 10^4 L_{\odot}$ for $M_{\text{WD}} = 1.2 M_{\odot}$,

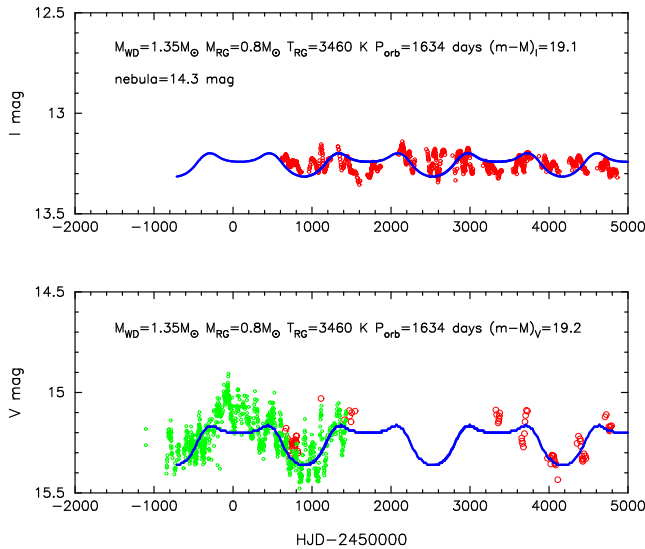


FIG. 3.— I and V light curves of SMC 3. Solid curves denote our model light curves for a $1.35 M_{\odot}$ WD and $0.8 M_{\odot}$ RG. The original temperature of the RG (i.e., the temperature on the non-irradiated surface), T_{RG} , is the only parameter determined from light curve fitting in V band. We add a nebular emission of $m_I = 14.3$ to fit the I band data. The I and V data were taken from OGLE II/III (red open circles) and MACHO (small green open circles). Our light curve model reproduces well the long-term variation in the V magnitude as well as the very small dynamic range (~ 0.1 mag) of I magnitude variation. Irregular deviation from our model, especially in the I magnitude, may originate from the RG pulsation, possibly in a higher overtone mode, which our model does not include.

$L_{\text{WD}} = 3.34 \times 10^4 L_{\odot}$ for $M_{\text{WD}} = 1.1 M_{\odot}$, and $L_{\text{WD}} = 3.02 \times 10^4 L_{\odot}$ for $M_{\text{WD}} = 1.0 M_{\odot}$. We also assumed the RG mass to be $M_{\text{RG}} = 0.8, 1.0, 1.5$ and $2.0 M_{\odot}$. SMC3 is located in the direction of a dense H I cloud of $N_{\text{H}} = 4 \times 10^{21} \text{ cm}^{-2}$ (Kahabka & Pietsch 1996), but SMC3 is in front of this cloud, because the column density derived from spectral analysis of supersoft X-rays is much smaller than this value ($N_{\text{H}} \sim \text{several} \times 10^{20} \text{ cm}^{-2}$: Orio et al. 2007; Sturm et al. 2011). Therefore, we adopted $E(B - V) = 0.099$, a distance modulus of 18.91 (a distance of 60.6 kpc), $A_I = 0.179$, and $A_V = 3.1 \times E(B - V) = 0.31$ after Hilditch et al. (2005).

Figure 3 shows the OGLE-II (Udalski et al. 1997) and OGLE-III¹ (Udalski et al. 2008) I and V bands as well as the MACHO² blue band light curve. The MACHO light curve was shifted in magnitude to match OGLE’s V magnitude. This figure shows long-term variations in the I and V magnitudes, both of which are superposed with short pulsational variations of the RG.

Our model light curves are shown in Figure 3 for a $1.35 M_{\odot}$ WD and a $0.8 M_{\odot}$ RG. When the RG is in front of the WD ($\phi \sim 0.0$), we see only the original surface of the RG, where the magnitudes are faintest. On the other hand, when the RG is on the far side of the orbit ($\phi \sim 0.3 - 0.7$), we see the irradiated bright hemisphere of the RG. Thus, the light curve shows a wide dip. Secondary minima exist, as clearly shown in our model I light curve. They are due to ellipsoidal variation (a double peak in one orbital period) of a lobe-filling companion. Here we assume that only the RG contributes to

¹ <http://ogle.astrouw.edu.pl/>

² <http://www.macho.unu.edu.au/>

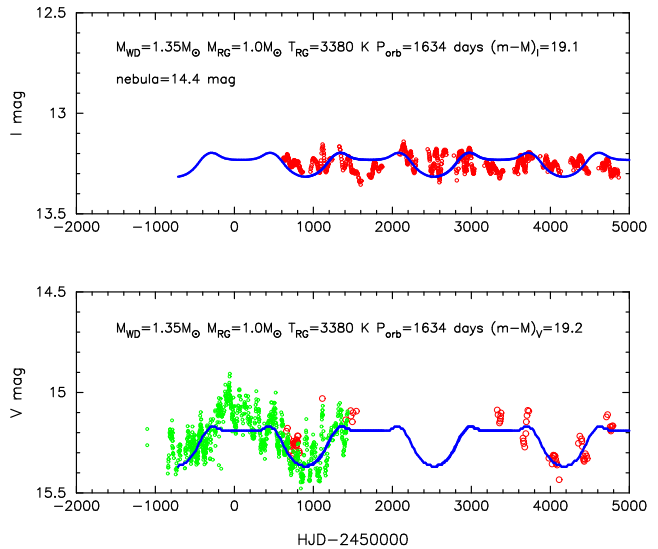


FIG. 4.— Same as Figure 3, but for a $1.0 M_{\odot}$ RG. We added nebular emission of $m_I = 14.4$ to fit the I band data.

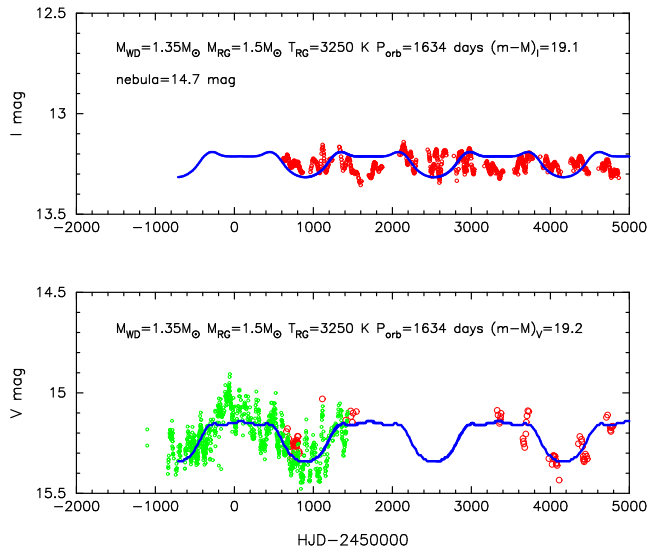


FIG. 5.— Same as Figure 3, but for a $1.5 M_{\odot}$ RG. We added nebular emission of $m_I = 14.7$ to fit the I band data.

the V band emission, not the nebulae, the contribution of which is discussed later. We found that the RG surface temperature of the non-irradiated side $T_{\text{RG}} = 3460$ K yields a good result in fitting with the V light curve. To fit the I band light curve, we had to assume a nebular contribution of $m_I = 14.3$.

If we assume no nebular contribution to I , we need to assume a higher temperature, $T_{\text{RG}} = 3700$ K, to obtain a good result. This may be explained if we are observing different “photospheres” of the RG envelope at different wavelengths. When we observe the I magnitude, we may see a deeper region where the temperature is higher. Another possible explanation is contamination by emission from the cool tail. The tail may contribute to the I band, but not the V band, reducing the temperature difference between different bands. Although the I band is contaminated by semiregular pulsations, our I light curve adequately reproduces the very small dynamic range (~ 0.1 mag) of the observed light curve.

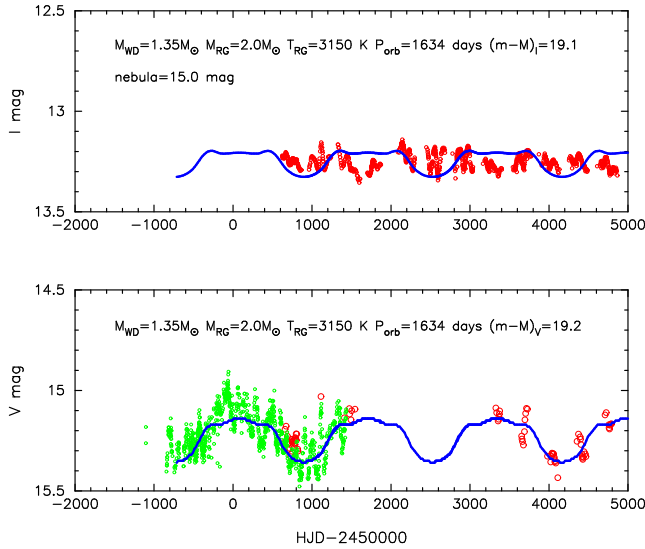


FIG. 6.— Same as Figure 3, but for a $2.0 M_{\odot}$ RG. We added nebular emission of $m_I = 15.0$ to fit the I band data.

Figures 4–6 show similar model light curves for a $1.35 M_{\odot}$ WD with different RG masses, i.e., $M_{\text{RG}} = 1.0, 1.5,$ and $2.0 M_{\odot}$. For a higher RG mass, we need to assume a lower RG surface temperature in order to obtain a similar magnitude. For a more massive RG, we obtained a larger separation a , and thus a larger effective Roche lobe radius (see Table 1). Therefore, we had to assume a lower temperature in order to obtain a similar magnitude. For each model, we assume a nebular contribution of $m_I = 14.3\text{--}15$ mag.

As in the previous section, the RG pulsation is not a fundamental mode, but possibly exists in higher overtones, which is consistent with the irregular pulsation behavior at small amplitude (~ 0.05 mag). These pulsations are not included in our theory, so we cannot reproduce the complicated I band variations. Instead, it is important that our light curve model reproduces the upper and lower limits of the I magnitude around the mean value by the same model that reproduces the long-term variation in the V band. In this sense, we may conclude that our model is consistent with both the V and I observations.

In Figures 3–6, the V magnitude is reproduced well by all of our theoretical models, whereas the I magnitude may be better reproduced by a low-mass RG companion. As shown in the previous subsection, $T_{\text{RG}} = 3700 \pm 100$ K is quite consistent with the pulsation theory, so we prefer a $0.8 M_{\odot}$ RG model to the others.

We also calculated V and I light curves for different masses of the WD, i.e., $M_{\text{WD}} = 1.2, 1.1,$ and $1.0 M_{\odot}$, which are more or less similar in both the V and I magnitudes (Figures 7, 8, and 9, respectively). Because both the I and V light curves are contaminated by irregular RG pulsations, we cannot determine which is the best fit to the observation. Thus, we could not determine the WD mass (or constrain the range of the WD mass) using only these light curve fittings.

The outer part of the hot thin nebula around the WD could contribute to the V band because it has a large volume even though it has very low emissivity. Part of the cool RG tail could also contribute to the V band if it is ionized by irradiation. Thus, we calculated an additional

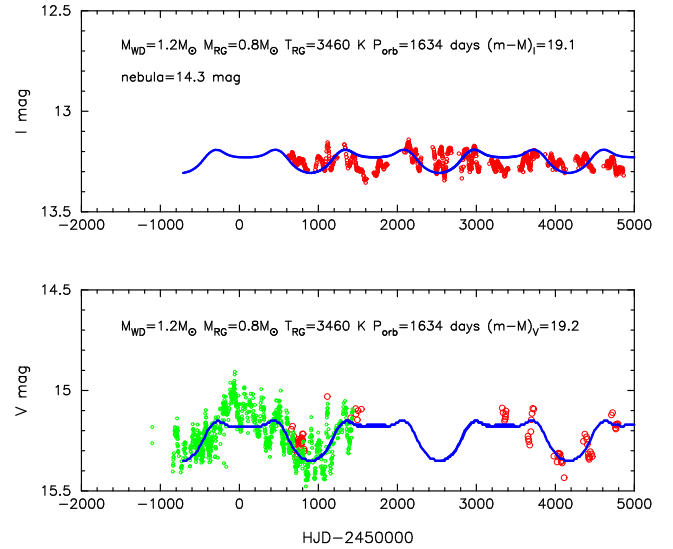


FIG. 7.— Same as Figure 3, but for a $1.2 M_{\odot}$ WD.

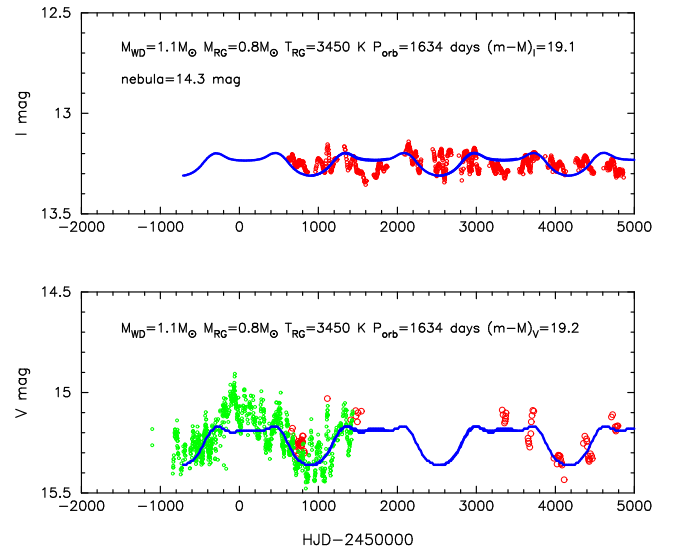


FIG. 8.— Same as Figure 3, but for a $1.1 M_{\odot}$ WD.

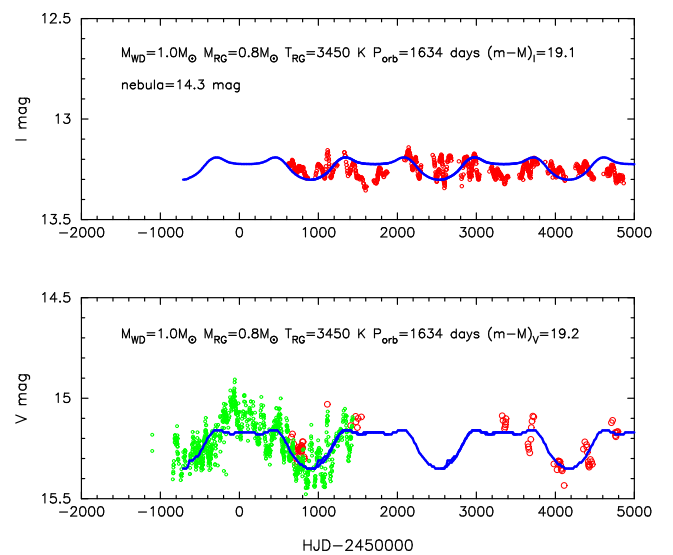


FIG. 9.— Same as Figure 3, but for a $1.0 M_{\odot}$ WD.

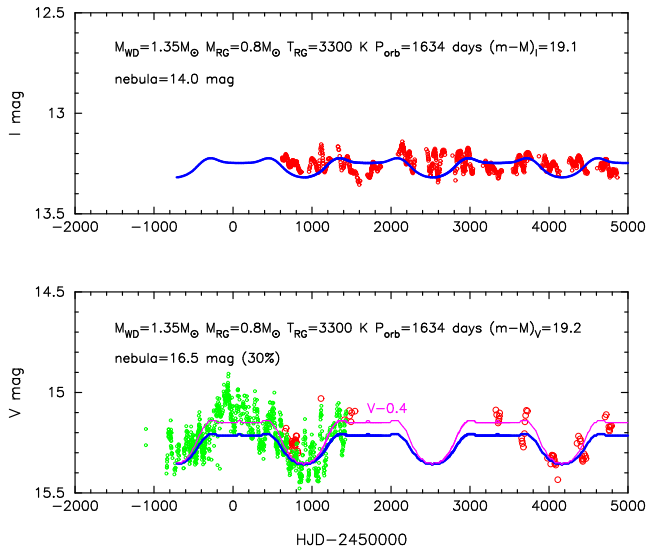


FIG. 10.— Same as Figure 3, but with nebular emission of $m_V = 16.5$ and $m_I = 14.0$ (thick solid blue lines). Thin solid magenta line denotes the original V magnitude (without nebulosity) shifted upward by -0.4 mag. The nebular emission of $m_V = 16.5$ corresponds to about 30% of the original luminosity. The calculated eclipses become too shallow to reproduce the observation.

light curve model in which the nebular contribution to the V band is as much as 30% of that of the RG. Figure 10 shows such a case for a pair of $1.35 M_\odot$ WD and $0.8 M_\odot$ RG. For example, if the nebular emission amounts to 30% of the RG luminosity in the V band, we obtain a lower temperature of $T_{RG} = 3300$ K for the RG companion. The total V magnitude is shown by a blue line. To fit our model with the I magnitude at the same RG temperature, we must increase the nebular contribution from $m_I = 14.3$ to $m_I = 14.0$. If we compare this model with Figure 3, the amplitude between minima and maxima becomes smaller in the V band, which is inconsistent with the observations. Therefore, we may say that the nebular contribution is probably less than $m_V > 16.5$.

In many symbiotic stars, the I and V band magnitudes are strongly contaminated by nebular emission (Nussbaumer & Vogel 1987; Skopal et al. 1998; Skopal 2005; Skopal et al. 2009). In SMC3, however, the companion RG is a very bright AGB star. This explains why the nebular contributions in I and V are rather small.

In our V light curve fitting, we use the ephemeris

$$\text{MJD}_{\min,V} = 49280 + N \times (1634) \text{ days.} \quad (2)$$

This is consistent with those of $\text{JD}_{\min} = 2449360 + N \times (1600 \pm 140)$ days by Kahabka (2004), and $\text{MJD}_{\min,B} = (49242 \pm 9) + N \times (1647 \pm 24)$ days by Sturm et al. (2011).

Periodic variations similar to those of SMC3 were observed in YY Her, a symbiotic binary of $P_{\text{orb}} = 590$ days. The RG fills its Roche lobe, and its hemisphere toward the WD is heated by irradiation. Mikolajewska et al. (2002) showed that the periodic change in the $UBVRI$ magnitudes can be described by a combination of ellipsoidal and sinusoidal changes. The RG radiation dominates in longer wavelength bands among $UBVRI$, so the variation can be represented well by ellipsoidal changes. On the other hand, the nebular continuum dominates in shorter wavelength bands, so the light curve shows a single minimum in one orbital period. These charac-

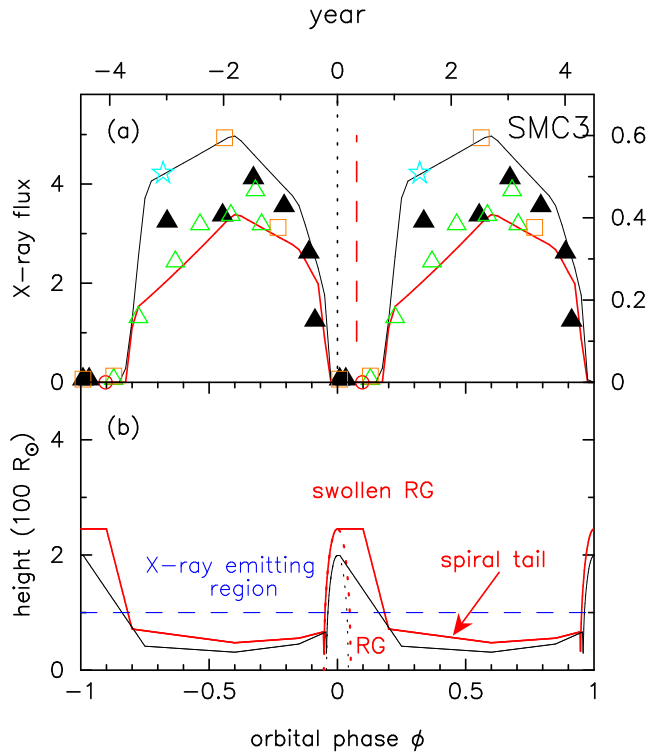


FIG. 11.— (a) X-ray light curve of SMC3. Data are taken from Sturm et al. (2011). Filled triangles: *ROSAT* PSPC. Open triangles: *ROSAT* HRI. Open circles: *Chandra*. Open squares: *XMM-Newton*. Stars: *Swift*. The supersoft X-ray flux (0.2–1.0 keV) is in units of $10^{-12} \text{ erg cm}^{-2} \text{ s}^{-1}$ (left ordinate). Solid lines indicate model light curves of X-ray eclipses; Model 1 for $R_{RG} = 245 R_\odot$ (thick red line), Model 2 for $R_{RG} = 199 R_\odot$ (thin black line). Right ordinate indicates the ratio of the calculated X-ray flux to the original value due to partial/total eclipse by the RG and its tail. Vertical dashed line indicates the central time of X-ray total eclipses for both Model 1 and Model 2 ($\phi = 0.075$). (b) Height of the RG and its tail from the orbital plane. Model 1 (thick red line), Model 2 (thin black line). Red and black dotted lines denote the RG surface in Models 1 and 2, respectively. Horizontal dashed line indicates the radius of the X-ray-emitting sphere around the WD.

teristic properties are already shown in our model light curves for SMC3. Figures 3–6 show that the I magnitude variations have double peaks whereas the V light curves display a single eclipse because the secondary minimum is compensated by extra radiation from the irradiated side of the RG.

4. X-RAY LIGHT CURVE

4.1. A Wide X-ray Eclipse

Figure 11a shows the X-ray fluxes of SMC3 against the orbital phase superposed for five orbital periods, the data for which are taken from Sturm et al. (2011), assuming the ephemeris and period determined by Equation (2) in Section 3. The same data are repeated for two orbital cycles. This X-ray light curve shows the following characteristic properties.

- (1): The X-ray eclipse is so wide that it spans $\Delta\phi \sim 0.15\text{--}0.3$ of the orbital phase represented by Equation (2).
- (2): The central time of X-ray eclipses is at $\phi \sim 0.1$, i.e., ~ 150 days after $\phi = 0.0$ as determined by

Equation (2), i.e., as determined from the long-term V variation.

- (3):** The eclipse has an asymmetric shape; the ingress is much steeper than the egress.

Regarding property (1), the eclipse duration is not unusually long among symbiotic stars. The duration depends on the wavelength because of absorption/scattering by surrounding material (RG winds) outside the RG photosphere. For example, in the symbiotic nova PU Vul ($P_{\text{orb}} = 13.5$ years), optical eclipse lasts $\Delta\phi = 0.07$, which is longer than the RG geometrical eclipse $\Delta\phi = 0.044$ because of TiO atmospheric absorption (Kato et al. 2012). At UV wavelengths region, its eclipse duration is even longer because of Rayleigh scattering as $\Delta\phi > 0.14$ (up to 0.27) (Tatarnikova & Tatarnikov 2009; Kato et al. 2011).

Regarding property (2), Sturm et al. (2011) already reported that the X-ray minimum comes 140 days after the V magnitude minimum. They noted this as B instead of V , but the MACHO blue is closer to yellow than B (Bessel & Germany 1999). They attributed this difference between the minima to a possible error in the V magnitude minimum due to the short observing period of MACHO (about 1.5 orbital periods). We see, however, a clear difference between the X-ray mid-eclipse and V magnitude minima because we determine the ephemeris from 3.5 orbital periods as shown in Figures 3–9.

All of these properties are consistent with an eclipse by an M giant companion swelling over the Roche lobe on the trailing side of the binary orbit, as was already been suggested in the symbiotic star SY Mus (Dumm et al. 1999; Pereira et al. 1995). The RG cool winds form a thick envelope, which tends to flow out mainly backward (on the trailing side of the RG) owing to orbital motion. As a result, SY Mus shows a wide eclipse in the UV continuum ($\phi \sim 0.9$ to ~ 1.18 , i.e., $\Delta\phi = 0.28$), which is much wider than the geometric eclipse by the RG companion itself ($\Delta\phi = 0.074$). Moreover, the UV 1325 Å continuum shows an asymmetric eclipse in which the ingress is steeper and closer to the mid-eclipse than the egress. This property is the same as property (3) of SMC3. Dumm et al. (1999) analyzed the UV spectrum and concluded that these eclipse properties are naturally explained by obscuration of the UV flux by a thick neutral hydrogen cloud (N_{H} from 10^{23} cm^{-2} to $> 10^{25} \text{ cm}^{-2}$) surrounding the RG.

Because the X-ray eclipse of SMC3 shows similar properties, we suppose that it is also caused not only by the RG companion itself, but also by a thick atmosphere surrounding the RG. In other words, properties (1)–(3) above are evidence of eclipses caused by a companion star swelling over the Roche lobe on the trailing side of the binary orbit (see Figure 2).

4.2. Circumbinary Configuration

For the X-ray emitting region, we simply assume a spherical hot nebula of radius R_{NE} centered on the WD. The WD itself emits stronger X-rays than the surrounding nebula, but the WD is believed to be always obscured by a neutral hydrogen cloud surrounding the binary in the orbital plane. Therefore, we observe only the extended X-ray source (blue region in Figure 2) which is

always partially occulted by the trailing tail from the RG. We will discuss the X-ray emitting region in Section 5.

We assume that the surface brightness of the X-ray emitting region is constant. This may not be a good approximation, especially if the hot nebular gas originates in the wind from the WD, the density of which decreases as r^{-2} , where r is the distance from the WD. Orio et al. (2007), however, suggested that their spectral analysis with CLOUDY favors a constant density distribution over an r^{-2} law. In that case, the surface emissivity (emissivity per unit area of the hot nebula in the line of sight) is close to constant rather than decreasing with increasing power of the distance from the WD. We suppose that if the X-ray flux is due to Thomson scattering with an optical depth of about 1 rather than thermal emission, the surface emissivity may not depend strongly on the distance from the WD. In this paper we do not discuss whether the X-ray flux is due to Thomson scattering, thermal emission of the hot plasma itself, or another cause, but, simply assume a uniform surface emissivity (a circular disk with a constant emissivity) as a first approximation.

Many numerical calculations show that cool RG winds (and also hot WD winds if present) form spiral structures around the binary (Sawada et al. 1986; Gawryszczak et al. 2002; Kim & Kim 2007; Edgar et al. 2008; Mohamed & Podsiadlowski 2012, and references therein). Ejected matter is highly aspherical, having a tendency to concentrate toward the orbital plane (Bisikalo et al. 2000; Gawryszczak et al. 2002; Edgar et al. 2008; Mohamed & Podsiadlowski 2012). In optical spectra of SMC3 (Morgan 1992; Mürset et al. 1996; Orio et al. 2007), Raman-scattered O VI lines indicate a significant amount of neutral material (Schmid 1996). Therefore, we suppose that SMC3 has a tail of neutral material concentrated in the orbital plane.

Figure 2 shows a schematic picture of our circumbinary model of X-ray eclipses. The RG is swollen to almost twice in its size in the direction opposite to the orbital motion and is followed by a long, geometrically thick tail surrounding the binary in the orbital plane. The shape of the RG and its tail is drawn schematically using information from numerical calculations by Sawada et al. (1986) and Mohamed & Podsiadlowski (2012), which show narrow spiral tails flowing from both stars. Mohamed & Podsiadlowski’s 3-D calculation showed that the outflowing matter is highly aspherical and concentrated in the orbital plane. The details of the mass distribution in the orbital plane do not affect our X-ray light curve model because we assume a total eclipse with an inclination of $i = 90^\circ$. Therefore, only the heights (perpendicular to the orbital plane) of the RG and tail are important in our X-ray light curve modeling, which we use to reproduce the X-ray light curve. We suppose that this tail is composed of neutral hydrogen, which is opaque only to supersoft X-ray photons but transparent to optical photons. As shown later, the radius of the X-ray emitting region $R_{\text{NE}} = 100 R_{\odot}$, which is about half of the RG radius. This ratio is roughly consistent with the mass distribution around the WD in the 3-D calculation of binary mass outflow (Mohamed & Podsiadlowski 2012), although their binary parameter differs from ours.

Such neutral hydrogen material, opaque to X-rays but

transparent to optical photons, was reported in the recurrent nova U Sco (Ness et al. 2012). In the supersoft X-ray phase followed by the 2010 outburst, U Sco temporarily showed irregular rectangular-shaped variations in the X-ray flux, whereas the UV and blue light curves showed a smooth eclipse. Ness et al. (2012) explained this X-ray variation as occultations of an extended X-ray region due to Thomson scattering by several blobs of neutral hydrogen moving in front of the X-ray emitting region. These blobs obscured supersoft X-rays but were transparent to UV/blue optical photons. In their analysis, the X-ray emitting region extends beyond the binary orbit (the orbital period is $P_{\text{orb}} = 1.23$ days, and the separation is $a = 6.5R_{\odot}$), and the blob sizes (0.73 – $1.1 R_{\odot}$) are comparable to that of the companion MS star ($R_{\text{MS}} = 2.1 R_{\odot}$). Because SMC3 is a wide binary ($P_{\text{orb}} = 1634$ days, $a = 700$ – $1000 R_{\odot}$ as tabulated in Table 1) and its SSS phase lasts much longer than that of U Sco (which lasts only 15 days), the circumstellar matter could be much more massive and extend to a much larger size than in U Sco.

In this paper, we assumed that the eclipse is essentially total; i.e., the X-ray emitting region (radius R_{NE}) is completely covered by the RG, although weak X-ray fluxes ($< 1/20$ of the X-ray high state) have been observed (Sturm et al. 2011). We regard these weak X-rays as light scattered by tenuous plasma widely distributed beyond the radius $R_{\text{NE}} (= 100 R_{\odot})$. This assumption does not affect our light curve modeling because the scattered light is very faint.

4.3. Model X-Ray Light Curve

Our model, which reproduces the observed X-ray variation, is shown in Figure 11. The orbital phase $\phi = 0.0$ is defined as when the RG is in front of the WD. The theoretical X-ray light curve is calculated from the area of the X-ray emitting region occulted by both the RG and its tail at a given orbital phase. Model 1 (denoted by a thick red line) assumes a greatly swollen RG with a thick (i.e., taller) tail and reproduces the lowest X-ray flux ever observed. On the other hand, Model 2 (denoted by a thin black line) assumes a smaller RG with a thin tail and reproduces the highest ever observed X-ray flux. The geometrical thickness of the tail is shown in Figure 11b, and its minimum height is listed in Table 2.

We found that an RG radius of 200 – $280 R_{\odot}$ is consistent with the ingress steepness, the value of which depends weakly on R_{NE} and the height of the tail. The nebula size of $R_{\text{NE}} = 100 R_{\odot}$ may be a bit large, but it cannot be a point source compared with the RG because the ingress shows a finite slope that is not perpendicular.

Outside of total eclipses (i.e., at the orbital phase $\phi \sim 0.3$ – 0.8), the X-ray data are scattered, as shown in Figure 11a; this represents real variations between different orbital cycles or is attributed to possible errors in the conversion factor between different satellites (Sturm et al. 2011). If this is a real variation, different X-ray fluxes are attributed to different shapes (heights) of the RG tail. Because the RG is pulsating with a period of 110 days, the mass-loss rate of the cool wind could vary with time, in addition to exhibiting possible long-term irregular variations. Thus, the RG tail naturally has different thicknesses (heights) at different times. (Note that periodic variations in the tail shape are observed in a 3-D

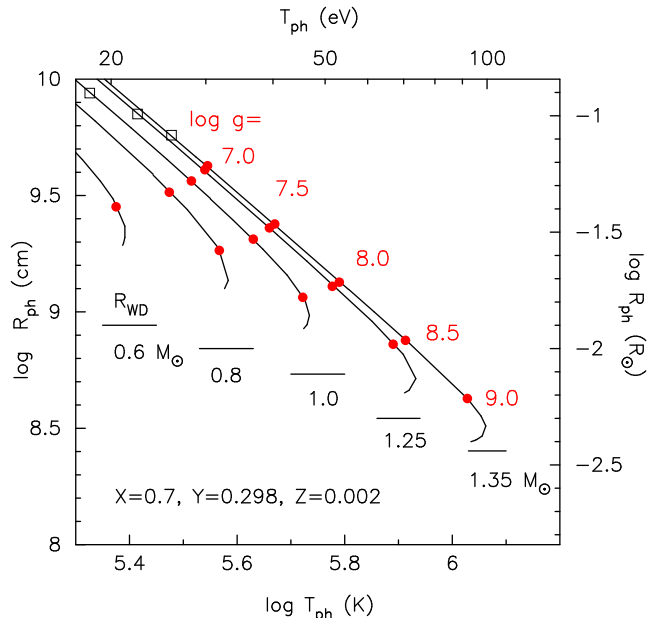


FIG. 12.— Photospheric radius versus photospheric temperature of our envelope models for WDs with masses of 0.6 , 0.8 , 1.0 , 1.25 , and $1.35 M_{\odot}$. The chemical composition of the envelopes is assumed to be $X = 0.7$, $Y = 0.298$, and $Z = 0.002$. Red filled circles indicate places at $\log g = 7.0$, 7.5 , 8.0 , 8.5 , and 9.0 . Optically thick winds occur in the region left of open square. No optically thick winds are accelerated by the 0.6 and $0.8 M_{\odot}$ WDs because of low metallicity in the SMC. Short horizontal bars indicate the Chandrasekhar radii corresponding to each WD mass.

calculation of the mass outflow from Mira with a periodically changing mass-loss rate having a period of 332 days: Mohamed & Podsiadlowski 2012). This explains the short-term variation in the X-ray flux as well as the differences among orbital periods. Note that the combination of the RG size and geometrical thickness (height) of the tail is not unique. We determined the tail height relative to $R_{\text{NE}} = 100 R_{\odot}$. If we adopt a smaller R_{NE} , for example, a similar X-ray light curve is obtained with the tail height multiplied by $R_{\text{NE}}/(100 R_{\odot})$ to the present models. The detailed distribution of circumbinary matter in the azimuthal and radial directions on the orbital plane does not affect our X-ray eclipse light curve model because only the height of the tail at a given orbital phase is important for determining the X-ray flux.

Figure 11a also indicates the central time of the X-ray total eclipse by a dashed line, according to the ephemeris determined from the V magnitude minimum. The X-ray mid-eclipse comes 123 days after $\phi = 0.0$ determined from the minima in the V light curve.

5. DISCUSSION

Figure 12 gives the photospheric radius versus the photospheric temperature for WDs of different masses with steady hydrogen-shell-burning. The chemical composition of the envelope is assumed to be $X = 0.7$, $Y = 0.298$, and $Z = 0.002$. The numerical method is the same as that in Kato (1999) and Nomoto et al. (2007). In the region to the left of the open squares, optically thick winds occur and absorb supersoft X-rays. In the region to the right of the open squares, the WD envelope is in hydrostatic equilibrium, which corresponds to a SSS phase. The lowest end of each line (i.e., the smallest WD radius) corresponds to the point at which hydrogen burn-

ing is extinguished. Orio et al. (2007) and Sturm et al. (2011) obtained an X-ray temperature for SMC3 as soft as 30–50 eV. If this temperature corresponds directly to the photospheric temperature, the radius of the photosphere is less than $0.1 R_{\odot}$, much smaller than the radius of the hot nebula, $R_{\text{NE}} = 100 R_{\odot}$. This is consistent with our assumption that the WD is always totally obscured by the RG and its long tail, and we see only X-rays scattered by the hot nebula.

This figure also shows the positions of the WD envelopes corresponding to surface gravities of $\log g=7.0, 7.5, 8.0, 8.5,$ and 9.0 , where $g = GM_{\text{WD}}/R_{\text{ph}}^2$ is the photospheric gravity. There are no envelope solutions corresponding to $\log g=8.5$ and 9.0 for $M_{\text{WD}} \lesssim 1.0 M_{\odot}$. Orio et al. (2007) suggested a large gravity of $\log g \sim 9.0$ and a low temperature of 36–47 eV on the basis of X-ray spectral fitting. Such a large gravity corresponds, in our WD envelope models, to a very massive WD ($\gtrsim 1.3 M_{\odot}$) with a small radius, and also a much higher temperature ($\gtrsim 100$ eV) as shown in Figure 12. The origin of this discrepancy is unclear.

On the basis of Orio et al. (2007), we assumed that the WD is surrounded by a very hot nebula, which scatters X-rays from the WD. We estimate the density of the hot plasma from the coronal lines. In principle, the electron density in the coronal region should be close to the critical density; e.g., the critical density for [Fe X] 6374 is $4.8 \times 10^9 \text{ cm}^{-3}$ (Nagao et al. 2001). In SMC3, both the [Fe X] 6374 and [Fe IX] 7892 lines are relatively strong and thus trace regions of high electron density, $N_e \sim 10^9$ – 10^{10} cm^{-3} . For a spherical emitting region of radius $R_{\text{NE}} = 100 R_{\odot}$ (fully ionized constant-density gas) the total mass of the nebula is estimated to be roughly 10^{-9} – $10^{-8} M_{\odot}$. The optical depth of the region in the line of sight is $\tau \sim \kappa \rho r = 0.004$ – 0.04 for the electron scattering opacity. Therefore, this region is optically thin, which is consistent with our assumption. However, these values are highly uncertain because of the simplified assumption.

We also estimate the temperature of this region. These coronal lines, [Fe X] and [Fe IX], have high ionization potentials (IPs), of 234 eV and 262 eV, respectively, and their presence indicates that the ionized matter is at a high temperature. Using the formula $T/(10^3 \text{ K}) \sim \text{maximum observed IP (eV)}$ (Mürset & Nussbaumer 1994), we obtain a temperature for the ionizing source of $T = (2\text{--}3) \times 10^5 \text{ K}$. This plasma temperature is consistent with the WD temperature estimated from X-ray spectrum analysis, 36–47 eV (4.2 – $5.5 \times 10^5 \text{ K}$) (Orio et al. 2007).

6. CONCLUSIONS

We estimated the radius of the RG and confirmed that it almost fills its Roche lobe. On the basis of this picture, we calculated the variations in orbital brightness including an irradiation effect and the geometrical effect of a tidally distorted companion. Our model reasonably reproduces the observed long-term I and V light

curves of SMC3. This again confirms that the RG almost fills its Roche lobe. Thus, the mass transfer rate from the RG to the WD could be high enough (\gtrsim a few times $10^{-7} M_{\odot} \text{ yr}^{-1}$) to maintain steady hydrogen-shell-burning on the WD (e.g., Nomoto et al. 2007), even though SMC3 is a long orbital period binary ($P_{\text{orb}} = 4.5$ years). This is quite consistent with the fact that SMC3 has been a steady SSS for at least 20 years.

Our main results are summarized as follows.

1. We presented I and V light curve models of SMC3. The observed magnitude variations can be reproduced by an irradiation of the RG by the hot WD as well as geometrical effects of the tidally distorted RG. This confirms that the RG component almost fills its Roche lobe, suggesting high mass transfer rates onto the WD, which maintain steady hydrogen-shell-burning on the WD.
2. We also presented an X-ray eclipse model in which an X-ray-emitting region is eclipsed by an RG companion swelling over the Roche lobe on the trailing side of the binary orbit. The X-ray-emitting region is highly ionized and extends to as large as $\sim 100 R_{\odot}$, scattering supersoft X-rays from the hot WD. This configuration reasonably reproduces the asymmetry of the X-ray eclipses, that is, steeper ingress than egress and the occurrence of the center of the X-ray eclipse about 120 days after the V minimum, as well as a very wide X-ray eclipse.
3. We also showed that our circumbinary matter configuration is consistent with various observed characteristics; our configuration is composed of a very hot nebula surrounding the WD and circumbinary matter (a spiral tail) of neutral hydrogen that always totally obscures the WD but partially occults the extended X-ray emission region. These configurations may be the key to the weakness of the supersoft X-ray flux in symbiotic systems.

We are grateful to the anonymous referee for useful comments that improved the manuscript. We also thank OGLE II/III for photometric data on SMC3. This paper utilizes public domain data obtained by the MACHO Project, jointly funded by the US Department of Energy through the University of California, Lawrence Livermore National Laboratory under contract No. W-7405-Eng-48, by the National Science Foundation through the Center for Particle Astrophysics of the University of California under cooperative agreement AST-8809616, and by the Mount Stromlo and Siding Spring Observatory, part of the Australian National University. This research was supported in part by the Grants-in-Aid for Scientific Research (22540254 and 24540227) from the Japan Society for the Promotion of Science, and by the Polish National Science Center grant no. DEC-2011/01/B/ST9/06145.

REFERENCES

- Bessell, M. S., Germany, L. M. 1999, *PASP*, 111, 1421
 Bessel, M. S., & Wood, P. R. 1984, *PASP*, 96, 247
 Bisikalo, D. V., Harmanec, P., Boyarchuk, A. A., Kuznetsov, O. A., & Hadrava, P. 2000, *A&A*, 353, 1009
 Cardelli, J.A., Clayton, G.C., & Mathis, J.S. 1989, *ApJ*, 345, 245

- Chiotellis, A., Schure, K. M., & Vink, J. 2012, *A&A*, 537, A139
- Dilday, B., Howell, D. A., Cenko, S. B., et al. 2012, *Science*, in press (arXiv:1207.1306)
- Di Stefano, R. 2010a, *ApJ*, 712, 728
- Di Stefano, R. 2010b, *ApJ*, 719, 474
- Dumm, T., Schmutz, W., Schild, H., & Nussbaumer, H. 1999, *A&A*, 349, 169
- Edgar, R. G., Nordhaus, J., Blackman, E. G., & Frank, A. 2008, *ApJ*, 675, 101
- Eggleton, P. P. 1983, *ApJ*, 268, 368
- Gawryszczak, A. J., Mikołajewska, J., & Różyczka, M. 2002, *A&A*, 385, 205
- Gilfanov, M., & Bogdán, A. 2010, *Nature*, 463, 924
- Hachisu, I. & Kato, M. 2001, *ApJ*, 558, 323
- Hachisu, I. & Kato, M. 2012, *Baltic Astronomy*, 21, 68
- Hachisu, I., Kato, M., & Nomoto, K. 1999a, *ApJ*, 522, 487
- Hachisu, I., Kato, M., Nomoto, K. 2010, *ApJ*, 724, L212
- Hachisu, I., Kato, M., Nomoto, K. 2012, *ApJ*, 756, L4
- Hachisu, I., Kato, M., Nomoto, K., & Umeda, H. 1999b, *ApJ*, 519, 314
- Hilditch, R. W., Howarth, I. D., & Harries, T. J. 2005, *MNRAS*, 357, 304
- Ita, Y., Tanabé, T., Matsunaga, N. et al. 2004, *MNRAS*, 347, 720
- Jordan, S., Schnutz, W., Wolff, B., Werner, K., & Mürset, U. 1996, *A&A*, 312, 897
- Kahabka, P. 2004, *A&A*, 416, 57
- Kahabka, P., & Haberl, F. 2006, *A&A*, 452, 431
- Kahabka, P., & Pietsch, W. 1996, *A&A*, 312, 91
- Kato, M. 1999, *PASJ*, 51, 525
- Kato, M. 2012, in *Binary Paths to the Explosion of Type Ia Supernova*, IAU Symp. 281 eds. R. Di Stefano & M. Orio, in press (arXiv:1110.0056)
- Kato, M., & Hachisu, I. 1994, *ApJ*, 437, 802
- Kato, M., Hachisu, I., Cassatella, A., & Gonzalez-Riestra, R. 2011, *ApJ*, 727, 72
- Kato, M., Mikołajewska, J., & Hachisu, I. 2012, *ApJ*, 750, 5
- Kim, H., & Kim, W.-T. 2007, *ApJ*, 665, 432
- Kučinskas, A., Hauschildt, P. H., Brott, I. & et al. 2006, *A&A*, 452, 1021
- Li, X.-D., & van den Heuvel, E. P. J. 1997, *A&A*, 322, L9
- Mikołajewska, J., Kolotilov, E. A., Shugarov, S. Yu., Yudin, B. F. 2002, *A&A*, 392, 197
- Mohamed, S., & Podsiadlowski, Ph. 2012, in *Asiago Workshop on Symbiotic Stars*, eds. A. Siviero, & U. Munari, *Baltic Astronomy*, 21, 88
- Morgan, D. H. 1992, *MNRAS*, 258, 639
- Mürset, & Nussbaumer, H. 1994, *A&A*, 586
- Mürset, U., Schild, H., & Vogel, M. 1996, *A&A*, 307, 516
- Mürset, U., Wolff, B., & Jordan, S. 1997, *A&A*, 319, 201
- Nagao, T., Murayama, T., & Taniguchi, Y. 2001, *PASJ*, 53, 629
- Nelson, T., Mukai, K., Orio, M., Luna, G. J. M., Sokoloski, J. L. 2011, *ApJ*, 737, 7
- Nelson, T., Donato, D., Mukai, K., Sokoloski, J., Chomiuk, L., 2012, *ApJ*, 748, 43
- Nielsen, M. T. B., Dominik, C., & Nelemans, G. 2012, *MNRAS*, submitted (arXiv:1207.6310)
- Nomoto, K., Saio, H., Kato, M., & Hachisu, I. 2007, *ApJ*, 663, 1269
- Nussbaumer, H., Vogel, M. 1987, *A&A*, 182, 51
- Orio, M., Nelson, T., Bianchini, A., Di Mille, F., & Harbeck D. 2010, *ApJ*, 717, 739
- Orio, M., Zezas, Z., Munari, U., Siviero, A., & Tepedelenlioglu, E. 2007, *ApJ*, 661, 1105
- Pereira, C.B., Vogel, M., & Nussbaumer, H. 1995, *A&A*, 293, 783
- Phillips, J. P. 2007, *MNRAS*, 376, 1120
- Sawada, K., Matsuda, T., & Hachisu, I. 1986, *MNRAS*, 219, 75
- Ness, J.-U., Schaefer, B. E., Dobrotka, A. et al. 2012, *ApJ*, 745, 43
- Schmid, H. M. 1996, *MNRAS*, 282, 511
- Schwarz, G. J., Ness, J-U., Osborne, J.P. et al., 2011, *ApJS*, 197, 31
- Skopal, A., 2005, *A&A*, 440, 995
- Skopal, A., Bode, M. F., Lloyd, H. M., & Drechsel, 1998, *A&A*, 331, 179
- Skopal, A., Sekereráš, M., González-Riestra, R., Viotti, R. F., 2009, *A&A*, 507, 1531
- Straižys, V., & Kuriliene, G. 1981, *Ap&SS*, 80, 353
- Sturm, R., Haberl, F., Greiner, J. et al. 2011, *A&A*, 529, 152
- Tatarnikova, A. A. & Tatarnikov, A. M. 2009, *Astronomy Reports*, 53, 1020
- Udalski, A., Kubiak, M., & Szymanski, M. 1997, *Acta Astronomica*, 47, 319
- Udalski, A., Szymanski, M. K., Soszynski, I., & Poleski, R. 2008, *Acta Astronomica*, 58, 69
- Vogel, M., & Morgan, D. H. 1994, *A&A*, 288, 842
- Wang, B., & Han, Z. 2012, *New Astronomy Reviews*, in press (arXiv:1204.1155)